Progress In Electromagnetics Research B, Vol. 10, 35–54, 2008

STATIC ECCENTRICITY FAULT DIAGNOSIS IN AN ACCELERATING NO-LOAD THREE-PHASE SATURATED SQUIRREL-CAGE INDUCTION MOTOR

J. Faiz and B. M. Ebrahimi

Center of Excellence on Applied Electromagnetic Systems
School of Electrical and Computer Engineering
University College of Engineering
University of Tehran
Tehran, Iran

Abstract—A no-load induction motor under static eccentricity is modeled using time stepping finite element (TSFE) method; current, torque, and speed signals of the motor are obtained by finite element method (FEM) and used for static eccentricity fault diagnosis and analysis. The frequency spectrum analysis of the stator current around fundamental frequency component is used to predict the static eccentricity. Noise, unbalanced magnetic pull (UMP) and arc occur during the starting of the faulty motor, therefore, performance of the motor over the period of starting up to the steady-state is investigated. It is shown that the rate of obtained signals from the constant permeability based analysis is very larger than that of the real case. It is indicated that in order to obtain accurate results the saturation must be taken into account in the analysis of the motor. Simulation results for a 3 hp, three-phase, 230 V, 36 stator slots induction motor with 28 rotor slots are given in this paper. Experimental results for the motor confirm the simulation results very well.

1. INTRODUCTION

Nowadays induction motors are widely used as the most common variable speed drive. The reasons are high reliability, high efficiency and good performance of the motor. Performance of a faulty motor disturbs the operation of the motor and also shortens its lifetime. Hence, diagnosis and detection of the faults make it possible to improve the performance of the motor and enlarge its life time [1]. The most important benefit of the fault diagnosis of the motor is that it makes

possible to estimate the approximate time of the damage and even to determine the part causing the fault by on-line analysis of the parameters variations. Meanwhile, the fault diagnosis methods form an important part of the basis of the modern management system such as artificial intelligent systems [2].

Many electrical and mechanical faults in the no-load operation of the motor lead to the eccentricity between the rotor and stator which show the importance of the eccentricity fault diagnosis. Performance of the motor due to the variations of the parameters (in faulty case) is predicted using the magnetic field distribution within the motor. Change of field distribution of a faulty motor, compared with that of the healthy motor, not only decreases the quality of the steady-state and dynamic performances of the motor, it also changes the parameters of the motor. It means that fault type may be diagnosed by simulation without carrying out costly tests.

Since 20 years ago, a continue effort has been devoted to the investigation of faults of ac drives which have been reported in [3]. There are different methods for analysis of a faulty motor; however application of these methods requires revision of the proposed assumptions and basic equations. For instance, when all harmonics contents of the air gap magnetic field are ignored, it is not expected that all the fault conditions of the stator winding or broken rotor bars be included in the model. Generally, the methods that use simplifying assumptions in the complicated electromagnetic and electro-dynamic equations of induction motor cannot include the fault conditions. Modeling and analyzing induction motor are important from steady-state and dynamic point of views. Different methods of analysis of induction motor that are capable to predict the behavior of the motor under eccentricity, broken or cracked rotor bars consists of: 1) magnetic equivalent circuit (MEC) method, 2) finite differences method (FDM), 3) winding function method (WFM) and 4) finite element method (FEM). Of course, there are some simple methods that capable to analyze induction motor in special conditions with rather low accuracy. Here full and precise methods are introduced.

In the MEC method, the equivalent magnetic circuits of all parts of the machine including the stator slot, rotor and stator yokes, air gap, stator windings and rotor bars are proposed. These individual magnetic circuits are then connected to each other based on the directions of the magnetic fluxes. The nodes of this circuit are the scalar magnetic potentials of different parts of the machine [4]. The MEC method is unable to take into account the effects of spatial harmonics due to the non-linearity of the ferromagnetic materials, topology of the machine, winding design and also time harmonics as a

result of inverter application. Complexities of the precise mathematical model of induction motors are always considered as the most difficult task in the fault diagnosis [5]. In fact, simple models such as MEC and $dq0$ (d and q are the direct and quadratic axes of the generalized model of the motor) are unable to diagnose electrical and mechanical faults precisely.

In the FDM, the governing differential equations of the motor are substituted by algebraic difference equations and they are then solved to obtain the magnetic field distribution within the motor. This method has an upper limit for the accuracy of the solutions.

The WFM uses electrical circuit coupling with magnetic circuit and compiles: the equations of the loop flux, stator winding currents, rotor bars current and motor voltages. These equations are expressed in respect to the stator windings and rotor bars resistances, and their self- and mutual-inductances. The next step in the application of the WFM is the computation of the mutual inductance between the stator windings and rotor bars. Winding function theory ignores the magnetic saturation. It is noted that the steady-state current, torque and speed in the cases of constant permeability and magnetic saturation are very close, because the operating point of induction motor places on the knee of the magnetization characteristic. However, induction motor saturates due to rapid changes of current and slip during the starting, and analysis under a constant permeability leads to very rapid changes of the current, torque and speed rate which differ with the practical case. This is more evident when induction motor under fault is analyzed. In the other methods that neglect the saturation, a large difference between the results for a constant permeability and real case exists. In spite of this, in the abnormal cases of a squirrel-cage rotor or due to other faults such as broken rotor bars or asymmetry of the air gap, estimation of the core losses is too difficult by the WFM.

Generally the above-mentioned methods have three basic deficiencies: First, variations of the magnetic permeance of air gap cannot be modeled when slots present. Second, locating saturation instantaneously in respect to the time average magnetic resistance cannot be modeled. Third, the rotor movement is not continuously recorded [2]. A proper and precise method for solving these problems is numerical method.

In decades 70th, the FEM progress leads to a wide application of the method in electrical engineering. In decades 80th, the FEM found applications in design, control and fault diagnosis of electrical machines. In spite of this, the full solution of magnetic field needs a very long computation time. This as well as configuration are the reasons for rare use of the FEM in the eccentricity diagnosis.

The reasons for long computation time in the motor with eccentricity are: 1) symmetry in the healthy induction motor, which reduces the computation time, non-exist in the faulty motor, 2) eccentricity of the air gap leads to considerable harmonics in the rotor current waveform. These harmonics do not take into account in the initial guesses of the machine analysis and this takes a long time [6].

The finite element method (FEM) has been widely used during the last two decades in the electromagnetic analysis [7–14]. In 1992, time stepping finite element (TSFE) method was used for modeling, analyzing and predicting induction motor performance [15, 16]. The method has taken into account actual features of the motor. Latter, between 1992 and 1999, this method was employed to analyze a faulty motor [2, 17–21]. However, TSFEM requires a large computer memory and long computation time. This is the reason for using a combination of TSFE and state-space method called time stepping finite element coupled state space (TSFESS) method for modeling and analyzing induction motor performance [5, 22]. The method was then used to predict and analyze an induction motor under fault and broken bar conditions. For simulation using TSFE method, the initial positions must be properly estimated, because numerical convergence of the winding currents depends on the good estimation of the initial positions. It is particularly true when an inverter-fed motor in no-load case is considered. Meanwhile, this method uses the FEM for computation of inductance and the rest of computations and analyzes are carried out using the state-space method [23–27]. There are two significant points in FE methods application in the analysis of induction motor under fault: firstly in the FE used for such analyzes, input of the equations is current density, secondly, the published papers have been so far dealt with the steady-state mode [28, 29]. Eccentricity in induction motor generates harmonic currents in the stator current and ignoring these harmonics leads to invalid results in the analysis of a faulty motor. It is necessary to note that the aim of fault diagnosis in induction motor in many researches have been to analyze the stator current for detection of the increase of the amplitude of the harmonic components or detection of new harmonic components due to the fault in the stator current. Therefore, the stator current must be estimated as the major variable in the analysis of a faulty induction motor. To solve this problem, TSFE-SS technique has been introduced in [23–27] where the winding current is calculated in a state-space and used as input of the FE equations; then inductances of the machine are calculated using FEM and used as input of the state-space equations. This process continues up to convergence which depends upon the proper estimate of the initial values of the rotor current and rotor

position. Secondly, FEM has been only used for inductance calculation and remaining computations and analyzes have been carried out in the state-space. This means duality in the precision of computations and analyzes which complicates the application of the FEM for analysis of the faulty induction motor. Therefore, the commercial software's capable to couple the electrical circuits and FEM, can be employed.

In this paper, modeling of faulty induction motor taking into account the spatial distribution of the stator windings, slots on both sides of the air gap and topology of the non-linear magnetic circuits is proposed. This removes the problems and short comes of the lumped parameter based models. Meanwhile, considering the non-linear behavior of the ferromagnetic materials in this modeling can eliminate the difficulty of the winding function in the fault analysis of the induction motor.

This paper uses the TSFE with voltage-fed, for analysis and detection of the static eccentricity fault. In this method, the inputs of the FE equations are the terminal voltages of the motor and stator phase current is the unknown value. So, all signals and variables have been calculated by FE with a very high accuracy and there is no need to couple the FEM and other environment such as analytical methods.

Following the simulation and computation of the stator current signal by TSFE method the spectrum analysis of the stator current over low frequencies (around fundamental component frequencies) has been carried out.

Since noise, unbalanced magnetic pull (UMP) and arc occur during the starting of the faulty motor, therefore, performance of the motor over the period of starting up to the steady-state is investigated. It is also shown in this paper that the variation rate of the signals obtained from the constant permeability based analyses are much larger than the relevant rates observed in results considering magnetizing curves. It is shown that in order to obtain accurate results the saturation must be taken into account when this analysis is carried out.

2. TRANSIENT ANALYSIS OF A FAULTY INDUCTION MOTOR

FEM can be used for steady-state analysis of induction motor under eccentricity fault. It is also possible to analyze the transient behavior of induction motor by the FEM. This is required in the control of induction motor in order to obtain the optimal time response.

Meanwhile, the transient analysis of the motor is required for on-line fault diagnosis of the motor. A voltage-fed three-phase induction

motor is analyzed from the starting up to the steady-state mode in which the continuous motion of rotor is proposed using TSFE method. The FE matrix equations, electric circuits equations and electromechanical equations are solved every step. The couple solver part of Opera-2d is used in order to allow the user to study the transient behavior of the motor.

There are three fundamental parts in the transient analysis of induction motor: 1) modeling of motor, 2) connecting electrical circuits and supply modeling and 3) electromechanical connections.

2.1. Modeling Squirrel-cage Induction Motor

The proposed three-phase squirrel-cage induction motor, with cross-section shown in Fig. 1, is modeled taking into account the properties of the various parts including stator, rotor, shaft, rotor bars and air gap. Table 1 summarizes the specifications of the proposed induction motor. Meanwhile, a special attention is paid to the moving parts of the motor, because magnetic forces and positions influence, in turn, the magnetic field within the motor. In the model, the voltage is applied as input and the total current is the unknown value. The transient equations of the external circuit that show the electrical supply and circuit elements are combined with the equations of the FEM. Also the motion equations are combined with the field equations of the FEM. Finally, in the moving electromagnetic systems, it is necessary to introduce the speed in the equations.

The equation which covers this section is as follows:

$$\nabla \times \left(\frac{1}{\mu}\vec{V} \times \vec{A}\right) + \sigma \left(\frac{\partial \vec{A}}{\partial t} - \vec{v} \times \left(\nabla \times \vec{A}\right)\right) = \vec{J} \tag{1}$$

Using a reference frame which is assumed constant under the study part, the relative speed v is expressed as follows:

$$\nabla \times \left(\frac{1}{\mu}\nabla \times \vec{A}\right) + \sigma \left(\frac{\partial \vec{A}}{\partial t}\right) = \vec{J} \tag{2}$$

In the FE analysis, such reference frame is created by placing a mesh on the surface of the moving part and movement or transformation occurs only within the elements that are placed around the moving element [30].

2.2. Connecting Electrical Circuits and Supply Modeling

All rotor bars and stator conductors that have been presented in the circuit model are shown using the real constants in the FEM.

Table 1. Specifications of the proposed three-phase induction motor.

Number of poles	4
Outer diameter of stator, inch	8.188
Inner diameter of stator, inch	4.875
Air-gap length, inch	0.013
Core length, inch	2.5
Shaft diameter, inch	1.357
Length of rotor slot, inch	0.532
Number of stator slots	36
Number of rotor slots	28
Rated voltage, V	230
Rated frequency, Hz	60
Rated power, hp	3
Skew	0.425

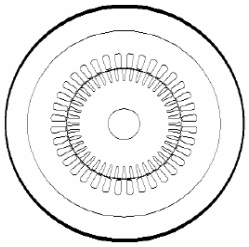

(a)

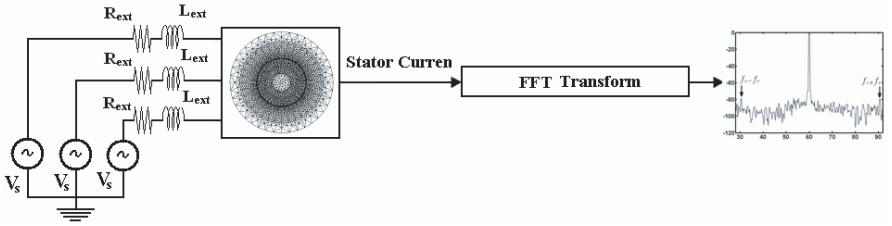

(b)

Figure 1. (a) Cross section of proposed induction motor and (b) Diagnosis of static eccentricity fault in induction motor.

Additional resistance and inductance place in series with the every phase of the winding. The induction motor is supplied by a three-

phase sinusoidal supply. Rotor bars in the relevant circuit are in parallel. Three stator windings of phases a, b and c have identical turns number and resistances. Three-phase symmetrical voltages are applied to the stator. The two-dimensional propagation equation is as follows:

$$\nabla \times \vec{v}\nabla \times \vec{A} = \vec{J} \tag{3}$$

where J and A are taken to be in z direction and independent of z. The current density is as follows:

$$\vec{J} = \sigma \frac{\vec{V_b}}{l} - \sigma \frac{\partial \vec{A}}{\partial t} + \sigma \vec{v} \times \vec{B} \tag{4}$$

where gradient of V_b in z direction has amplitude V_b/l. The first term in the right hand side of (4) shows the current density due to the power supply. The second term shows the induced current density and the third term indicates the produced current density by the series voltage. It is not practically possible to separate its different parts due to mathematical concept of (4). Therefore, the time-dependent magnetic propagation equation is as follows:

$$\nabla \times \vec{v}\nabla \times \vec{A} = \sigma \frac{\vec{V_b}}{l} - \sigma \frac{\partial \vec{A}}{\partial t} + \sigma \vec{v} \times \nabla \times \vec{A} \tag{5}$$

Using a reference frame which is considered constant in respect with the element under study, the relative speed v is zero and (5) is simplified as follows:

$$\nabla \times \vec{v}\nabla \times \vec{A} = \sigma \frac{\vec{V_b}}{l} - \sigma \frac{\partial \vec{A}}{\partial t} \tag{6}$$

For combining the circuit and field equations, it is necessary to calculate the total current of every conductor. This is done by integration of (6) over the cross-section of the conductor as follows:

$$i = \iint \left(\sigma \frac{V_b}{l} - \sigma \frac{\partial A}{\partial t} \right) dxdy \tag{7}$$

A matrix is used to represent a general circuit which has voltage source (V_b), impedance (Z) and inductance (L), where:

$$[V_b] = [Z][i] + [L]\frac{di}{dt} \tag{8}$$

There is a network equation per network "loop" and a component may be a member of more than one loop. The non-linear equation that can

relate the FE equations expressing the electromagnetic fields of the machine with the circuit equations is as follows:

$$[C][A \quad i]^T + [D]\left[\frac{\partial A}{\partial t} \quad \frac{\partial i}{\partial t}\right]^T = [P] \tag{9}$$

Solution of (9) gives magnetic potential vector $[A]$ and stator current $[i]$. $[C]$ and $[D]$ are the coefficients matrices and $[P]$ is the vector related to the input voltage. In the steady-state analysis of a on-load voltage-fed induction motor, after a very short time, the motor approaches the speed corresponding to the proposed load, in this case $[A]$ and $[i]$ are determined as follows:

$$[C][A \quad \mathrm{I}]^T + [D][j\omega A \quad j\omega \mathrm{I}]^T = [P] \tag{10}$$

where ω is the equivalent of input angular frequency.

2.3. Electromechanical Connections

The developed electromagnetic torque of the motor is as follows:

$$T_{em} = (L_{eff}/\mu_0) \int_\Gamma \left[\left(\vec{B} \cdot \vec{n}\right)(\vec{r} \cdot \vec{B}) - 0.5B^2(\vec{r} \times \vec{n})\right] d\Gamma \tag{11}$$

where, $\vec{n}$ is the unit vector normal to the contour, $\vec{r}$ is the vector pointing from the axis rotation to a point on the contour. The discrete developed electromagnetic torque is obtained as follows:

$$T_{em} = (2L_{eff}r^2/\mu_0) \sum_{i=1}^{n} B_{ri}B_{\theta i}\Delta\theta_i \tag{12}$$

where r is the radius of the contour, n is the number of elements passed the contour over a pole pitch, B_r and B_θ are the normal and tangential component of the magnetic flux density in each element respectively.

The induction motor motion equation can be expressed as follows:

$$\omega_r(t) = \frac{1}{J} \int (T_{em} - T_{load})\, dt \tag{13}$$

3. MAGNETIC FIELD ANALYSIS

Figure 2 presents the flux lines distribution within the healthy and faulty induction motor at the starting and steady-state operations. As

shown in Fig. 2(a), the reason for asymmetry distribution of the flux are the rapid changes of the slip at the starting and also eddy current in the rotor bars. When the motor approaches the steady-state mode, the flux distribution becomes symmetrical as shown in Fig. 2b. Fig. 2c presents the flux distribution within the faulty motor. There is also asymmetry due to the fault (Fig. 2d) in the steady-state operation. When the eccentricity occurs, the air gap field that consists of the fundamental component, stator and rotor mmf harmonics and stator and rotor slot permeances, will have new harmonic components due to the fault. Therefore, flux distribution in faulty motor under static eccentricity is distorted. This fact has been shown in Fig. 2a–Fig. 2d. In addition to the above-mentioned reasons for asymmetry distribution of the flux in the healthy motor, eccentricity injects harmonics currents in the current of the faulty motor.

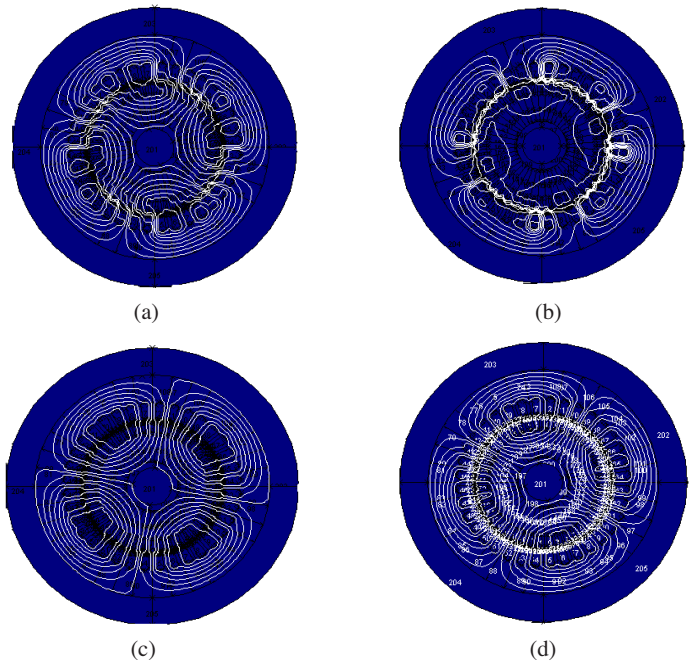

Figure 2. Flux distribution: (a) starting operation of healthy motor, (b) starting operation of faulty motor, (c) steady-state operation of healthy motor, (d) steady-state operation of faulty motor.

4. STATOR CURRENT ANALYSIS

Figure 3 and Fig. 4 show the time variations of an induction motor no-load current with constant permeability and considering magnetization characteristic for the healthy and faulty cases respectively. Comparison of Figs. 3(a), 3(b) with the corresponding Figs. 4(a), 4(b) indicates that the static eccentricity causes unbalance stator current. Also comparison of Fig. 3 and Fig. 4 shows that this unbalance current is very larger for the constant permeability case. The reason is the high saturation during the acceleration of the induction motor. If this saturation is ignored, the air gap flux density distribution will be very large. This is clearer when a fault occurs. Therefore, the rate of variations of the health and faulty induction motor are also very larger than that case in which the magnetization characteristic is included.

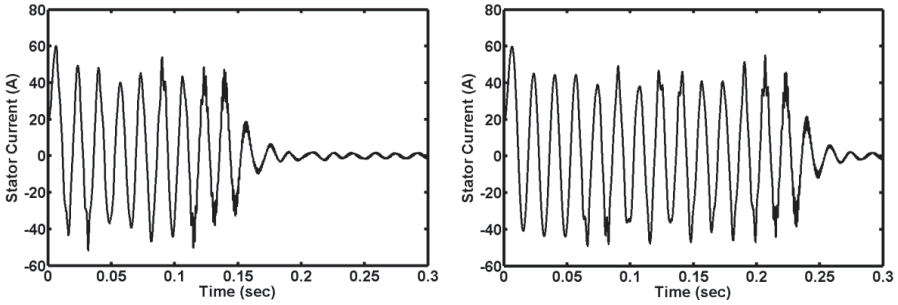

(a) (b)

Figure 3. Time variations of current of a no-load induction motor with constant permeability: (a) healthy motor, (b) motor with 41.37% static eccentricity.

As seen in Fig. 2, static eccentricity leads to asymmetrical magnetic flux distribution of the motor. Meanwhile, static eccentricity injects harmonics with particular frequencies into the air gap magnetic flux density distribution. These frequencies depend on the position and numbers of slots, static and dynamic degrees. Also rotating flux waves induce the currents with the same frequencies in the stator. Therefore, for static eccentricity diagnosis, a current spectrum analysis must be carried out.

5. SPECTRUM ANALYSIS OF STATOR CURRENT

The first stage of investigation is sampling the current or converting analog signal to digital signal. It is noted that the large rate of sampling makes the sampled close to the real signal. In such a case

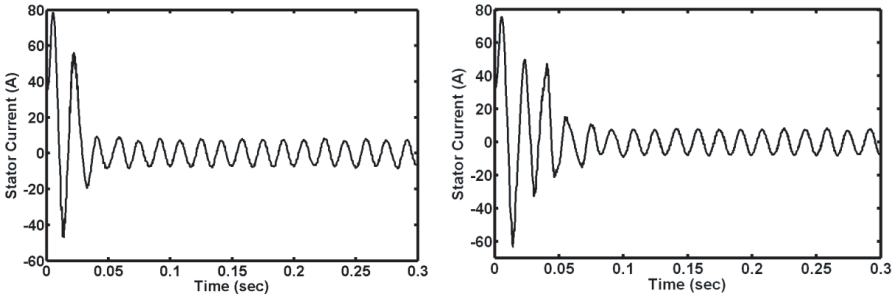

Figure 4. Time variations of current of a no-load induction motor considering magnetization curve: (a) healthy motor, (b) motor with 41.37% static eccentricity.

the data and processing will be higher. Considering the sampling method and according to the Nyquist law for sampling, the sampling frequency must be at least twice the maximum available frequency. Since the frequency components of the actual signals are distributed and generally the maximum frequency components are unknown, and also a limited spectrum of the signal is frequently proposed, in order to present the folding or similarity, a low-pass filter with cut off frequency equal to f_{cut} is used at the input. f_{cut} is determined based on the proposed frequencies at the input signal.

Under static eccentricity, many harmonics are injected to the stator current and amplitudes of the harmonic components are increased by fault increment. Therefore, for signal processing of the stator current of the healthy and faulty motor, spectrum analysis of the stator current signal is necessary Analysis of the stator current spectrum for diagnosis of the static eccentricity using harmonic components around the fundamental component, existing harmonics of the slot harmonics, called principle slot harmonic (PSH), are necessary for eccentricity fault diagnosis. Generally, equation due to the slot fundamental harmonic and harmonics connected to the static and dynamic eccentricities is as follows:

$$f_{eccentricity} = \{(KR \pm n_d)(1-s)/P \pm \eta\} f_s \tag{14}$$

where n_d is the eccentricity degree which is equal to zero for the static eccentricity and equal to 1, 2, 3, ... for the dynamic eccentricity depending on the eccentricity degree. K is an integer, P is the number of pole pairs, R is the number of rotor slots and η is the harmonic order 1, 3, 5, ... If $n_d = 1$, $K = 0$ and $\eta = 1$, (14) will be simplified

as follows:

$$f_{eccentricity} = f_{eccentricity}(0,\ 1,\ S,\ 1) = (1 \pm \frac{1-S}{P})f_s \tag{15}$$

$$f_r = \left(\frac{1-S}{P}\right) f_s \tag{16}$$

$$f_{eccentricity} = f_s \pm K f_r \tag{17}$$

where $K = \pm 1 \pm 2 \pm 3, \ldots$. These harmonics, located around the fundamental frequency of the supply are due to the mixed eccentricity. Therefore, the mixed eccentricity injects harmonic components with pattern $f_s \pm K f_r$ into the stator current. The fundamental harmonic is obtained for $K = 1$. These harmonics must be searched around the fundamental frequency component.

Figures 5(a) and 5(b) show the simulated and tested frequency spectrum of the stator current for a healthy motor. According to these figures, amplitudes of harmonic components $f_s - f_r$ and $f_s + f_r$ are -78 dB and -79 dB respectively. Referring to Figs. 6(a) and 6(b) confirms that a 41.37% static eccentricity increases the amplitudes of harmonics $f_s - f_r$ and $f_s + f_r$ to -55 dB and -57 dB respectively which can be used to diagnose the static eccentricity fault. Under static eccentricity fault, the air gap field, which includes the fundamental components of the stator and rotor flux, stator and rotor slot permeance produces more harmonic components because of the faults; consequently the fundamental harmonics of the slot in the phase current against the air gap asymmetry increases, so harmonic contents in the stator phases currents will be increased. Table 2 summarizes the sideband components at frequency $f_s \pm k f_r$ for the healthy and faulty motor under different static eccentricity degrees.

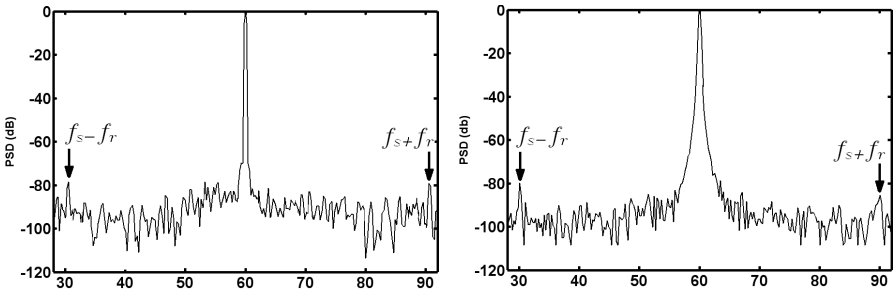

Figure 5. Normalized low-frequency line current spectra of healthy induction motor: (a) simulate, (b) experimental.

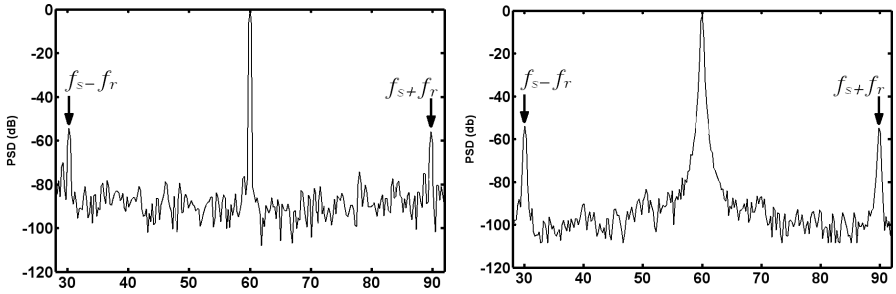

Figure 6. Normalized low-frequency no-load line current spectrum of induction motor with 41.37% static eccentricity: (a) simulated, (b) experimental.

Table 2. Amplitude of sideband components at frequency $f_s \pm k f_r$ for healthy and faulty motor in dB.

Static eccentricity degree (%)	$f_s - f_r$	$f_s + f_r$	$f_s + 2f_r$	$f_s + 3f_r$
0	−78	−79	−70	−89
10	−62	−65	−66	−85
20	−59	−62	−64	−83
30	−57	−60	−61	−80
40	−55	−57	−58	−77
50	−52	−55	−56	−75

6. ANALYSIS OF FAULTY MOTOR PERFORMANCE

Simulations are carried out for an unsaturated and saturated magnetic circuit of an no-load induction motor with different degrees of static eccentricities. In most available analyses of the eccentricity in induction motor, the saturation effect has been neglected, but a comparison of the analysis for two cases indicates that there are three large differences between the saturated and unsaturated cases.

In the healthy induction motor at stall, the input of the motor is the stator resistance and leakage reactance in series with the resistance and leakage reactance of the rotor. Consequently, the applied full voltage produces a very large starting current. Since at the beginning of the starting, speed fluctuations are very large, the slip varies severely and therefore the time variations of the torque have many ripples. However, by passing the time, it approaches the rated speed and slip

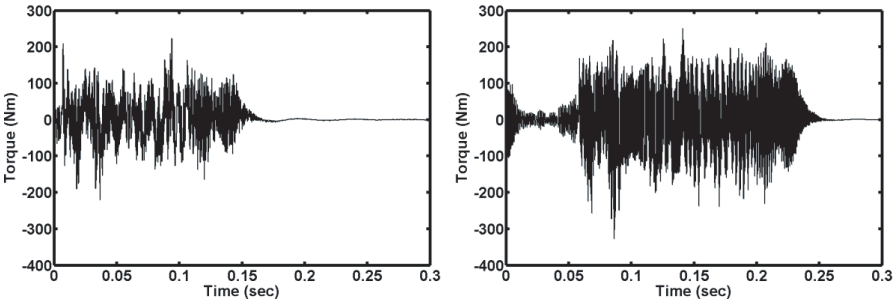

Figure 7. Time variations of torque of a no-load induction motor with constant permeability: (a) healthy motor, (b) motor with 41.37% static eccentricity.

tends to its rated value. At the same case, dc components appear in the torque/time profile. Time variations of the current will be sinusoidal with the rated amplitude. The increase of the harmonic components of the stator current increases the rate of the changes of electromagnetic torque compared with that of the healthy motor. Figs. 7 and 8 present these cases. Also simulation results show that the motor with different degrees of eccentricities approach more quickly the steady-state mode compared with the healthy motor. As shown in Figs. 3–6, this leads to a higher starting current compared with the healthy motor. The higher current in the eccentricity case generates a higher torque. The reason for increasing the starting torque is related to the increase of the mutual inductance between the stator and rotor. Consequently, the rate of energy and electromagnetic torque increase compared with that of the healthy motor. Fig. 9 shows the time variations of the speed in the above-mentioned degrees of the eccentricities. Comparison of the current, torque and speed curves in the two above cases shows the importance of including the saturation in the computations. If saturation is neglected, starting current as well as flux density will be high, this particularly clear in the teeth. Reduction of the reluctances of different parts of the stator and rotor and also their teeth lead to a considerable increase of the magnetic potential of the teeth and this causes a high starting torque. When saturation is included, core saturates due to the high starting current which in turn reduces the magnetization inductance and stator self-inductance.

So, reluctances of the stator and rotor teeth increase and magnetic potential and consequently starting torque decrease considerably. As shown in Figs. 8(a) and 8(b), the torque has less variations and amplitude compared with the linear magnetic circuit case. Also current

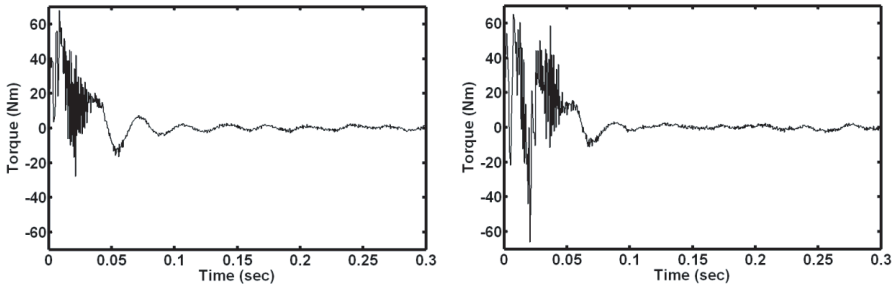

Figure 8. Time variations of torque of a no-load induction motor considering magnetization curve: (a) healthy motor, (b) motor with 41.37% static eccentricity.

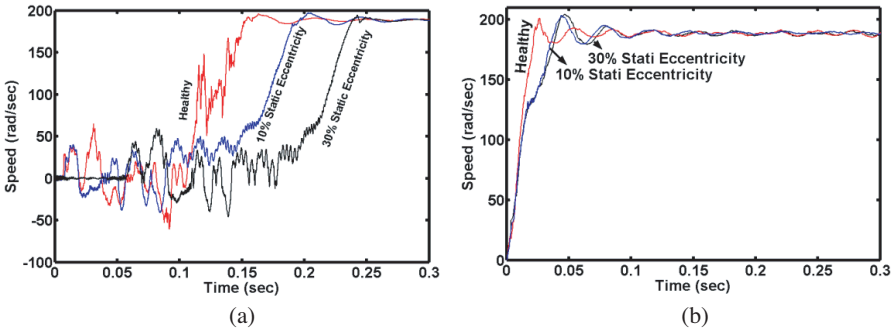

Figure 9. Time variations of speed of a no-load healthy and faulty induction motor: (a) constant μ, (b) considering magnetization curve.

(Figs. 4(a) and 4(b)), speed (Fig. 9(b)), characteristics show that, the variations are less compared with those obtained with constant permeability.

7. CONCLUSIONS

Induction motor under static eccentricity was studied using TSFE method where voltage supply was used as input of the FE computation part. This technique could solve the problems and complexities in application of FE with current density as input. All analyzes were carried using FEM which led to a very high precision.

Static eccentricity fault in induction motor was diagnosed using stator current spectrum analysis. It was shown that static eccentricity fault can inject large harmonics to the stator current; particularly

$f_s - f_r$ and $f_s + f_r$ harmonics were considerably increased. It was proved that the rate of the electromagnetic torque of the faulty motor is increased during the starting period compared with that of the healthy motor. This could largely increase noise and UMP in the motor. It was shown that the fault develops higher starting torque and at the same time it is more oscillatory, so the time of approaching the steady-state is shorter.

In order to indicate the influence of the saturation upon the analysis of the faulty induction motor, two constant and non-liner permeability were included in the paper. Finally it was shown that there is considerable difference between the analysis results for both cases.

List of Symbols

g uniform air gap length	A magnetic vector potential
v velocity	J_0 current density
σ electrical conductivity	l length in z direction
V_b applied voltage	B magnetic flux density
L_{eff} effective machine length	J inertia
ω_r angular speed	B_m damping factor
T_{em} electromagnetic torque	T_{load} load torque

REFERENCES

1. Bonnett, A. H. and G. C. Soukup, "Cause and analysis of stator and rotor failures in three-phase squirrel-cage induction motors," *IEEE Transactions on Industry Applications*, Vol. 28, No. 4, 921–937, Jul.–Aug. 1992.
2. Thomson, W. T., "On line current monitoring and application of a finite element method to predict the level of static air gap eccentricity in three-phase induction motors," *IEEE Transactions on Energy Conversion*, Vol. 13, No. 14, 347–354, Dec. 1998.
3. Benbuzid, M. E. H., "Bibliography on induction motors faults detection and diagnosis," *IEEE Transactions on Energy Conversion*, Vol. 14, 1065–1074, Dec. 1992.
4. Ostovcic, V., "A method for evaluation of transient and steady state performance in saturated squirrel cage induction machines," *IEEE Transactions on Energy Conversion*, Vol. 1, No. 3, 190–197, Sept. 1986.
5. Demerdash, N. A., J. F. Bangura, and A. A. Arkadan, "A time-stepping coupled finite element-state space model for induction

motor drives. I. Model formulation and machine parameter computation," *IEEE Transactions on Energy Conversion*, Vol. 14, No. 4, 1465–1471, Dec. 1999.

6. Stoll, R. L., "Simple computational model for calculating the unbalanced magnetic pull on a two-pole turbo generator due to eccentricity," *IEE Proc. Elect. Power Appl.*, Vol. 144, No. 4, 263–270, 1997.
7. Vaish, A. and H. Parthasarathy, "Analysis of a rectangular waveguide using finite element method," *Progress In Electromagnetics Research C*, Vol. 2, 117–125, 2008.
8. Zhou, X. and G. Pan, "Application of physical spline finite element method (PSFEM) to full wave analysis of wave guides," *Progress In Electromagnetics Research*, PIER 60, 19–41, 2006.
9. Qiu, Z. J., J. D. Xu, G. Wei, and X. Y. Hou, "An improved time domain finite element-boundary integral scheme for electromagnetic scattering from 3-d objects," *Progress In Electromagnetics Research*, PIER 75, 119–135, 2007.
10. Faghihi, F. and H. Heydari, "A combination of time domain finite element-boundary integral with time domain physical optics for calculation of electromagnetic scattering of 3-d structures," *Progress In Electromagnetics Research*, PIER 79, 463–474, 2008.
11. Sun, X. Y. and Z. P. Nie, "Vector finite element analysis of multicomponent induction response in anisotropic formations," *Progress In Electromagnetics Research*, PIER 81, 21–39, 2008.
12. Tai, C.-C. and Y.-L. Pan, "Finite element method simulation of photoinductive imaging for cracks," *Progress In Electromagnetics Research Letters*, Vol. 2, 53–61, 2008.
13. Zhou, X., "Physical spline finite element (PSFEM) solutions to one dimensional electromagnetic problems," *Progress In Electromagnetics Research*, PIER 40, 271–294, 2003.
14. Isaakidis, S. A. and T. D. Xenos, "Parabolic equation solution of tropospheric wave propagation using FEM," *Progress In Electromagnetics Research*, PIER 49, 257–271, 2004.
15. Demerdash, N. A. and P. Baldassari, "A combined finite element-state space modeling environment finite element-state space modeling environment for induction motors in the ABC frame of reference: The no-load condition," *IEEE Transactions on Energy Conversion*, Vol. 7, No. 4, 698–709, Dec. 1992.
16. Baldassari, P. and N. A. Demerdash, "A combined finite element-state space modeling environment for induction motors in the ABC frame of reference: The blocked-rotor and

sinusoidally energized load conditions," *IEEE Transactions on Energy Conversion*, Vol. 7, No. 4, 710–720, Dec. 1992.

17. Salon, S. J., M. J. DeBortoli, D. W. Burow, and C. J. Slavik, "Calculation of circulating current between parallel windings in induction motors with eccentric rotors by the finite element method," *Proceedings of ICEM'92*, 371–375, Manchester, UK, Sept. 15–17, 1993.
18. DeBortoli, M. J., S. J. Salon, D. W. Burow, and C. J. Slavik, "Effects of rotor eccentricity and parallel windings on induction machine behavior: A study using finite element analysis," *IEEE Transactions on Magnetics*, 1676–1682, Vol. 29, No. 2, 1993.
19. Arkkio, A. and O. Lindgren, "Unbalanced magnetic pull in a high-speed induction motor with an eccentric rotor," *Proceedings of ICEM'94*, 53–58, Paris, France, Sept. 5–8, 1994.
20. Arkkio, A., "Unbalanced magnetic pull in cage induction motors — Dynamic and static eccentricity," *Proceedings of ICEM'96*, 192–197, Vigo, Spain, Sept. 10–12, 1996.
21. Arkkio, A., "Unbalanced magnetic pull in cage induction motors with asymmetry in rotor structures," *IEE Conference Publication Proceedings of the 8th International Conference on Electrical Machines and Drives*, No. 444, 36–40, Sept. 1–3, 1997.
22. Bangura, J. F., F. N. Isaac, N. A. Demerdash, and A. A. Arkadan, "A time-stepping coupled finite element-state space model for induction motor drives. II. Machine performance computation and verification," *IEEE Transactions on Energy Conversion*, Vol. 14, No. 4, 1472–1478, Dec. 1999.
23. Bangura, F. and N. A. Demerdash, "Diagnosis and characterization of effects of broken bars and connectors in squirrel-cage induction motors by a time-stepping coupled finite element-state space modeling approach," *IEEE Transactions on Energy Conversion*, Vol. 14, No. 4, 1167–1176, Dec. 1999.
24. Bangura, J. F. and N. A. Demerdash, "Effects of broken bars/end-ring connectors and air gap eccentricities on ohmic and core losses of induction motors in ASDs using a coupled finite element-state space method," *IEEE Transactions on Energy Conversion*, Vol. 15, No. 1, 40–47, Mar. 2000.
25. Povinelli, R. J., J. F. Bangura, N. A. Demerdash, and R. H. Brown, "Diagnostics of bar and end-ring connector breakage faults in poly phase induction motors through a novel dual track of time-series data mining and time-stepping coupled FE-state space modeling," *Electric Machines and Drives Conference, 2001, IEMDC 2001, IEEE International 2001*, 809–813, 2001.

26. Povinelli, R. J., J. F. Bangura, N. A. Demerdash, and R. H. Brown, "Diagnostics of bar and end-ring connector breakage faults in poly phase induction motors through a novel dual track of time-series data mining and time-stepping coupled FE-state space modeling," *IEEE Transactions on Energy Conversion*, Vol. 17, No. 1, 39–46, Mar. 2002.
27. Bangura, J. F., R. J. Povinelli, N. A. Demerdash, and R. H. Brown, "Diagnostics of eccentricities and bar/end-ring connector breakages in poly phase induction motors through a combination of time series data mining and time-stepping coupled FE-state-space techniques," *IEEE Transactions on Industry Applications*, Vol. 39, No. 4, 1005–1013, Jul.–Aug. 2003.
28. Faiz, J. and B. M. Ebrahimi, "Mixed fault diagnosis in three-phase squirrel-cage induction motor using analysis of air-gap magnetic field," *Progress In Electromagnetics Research*, PIER 64, 239–255, 2006.
29. Faiz, J., B. M. Ebrahimi, and M. B. B. Sharifian, "Time stepping finite element analysis of rotor broken bars fault in a three-phase squirrel-cage induction motor," *Progress In Electromagnetics Research*, PIER 68, 53–70, 2007.
30. Pham, T. H., P. F. Wendling, S. J. Salon, and H. Acikgoz, "Transient finite element analysis of an induction motor with external circuit connections and electromechanical coupling," *IEEE Transactions on Energy Conversion*, Vol. 14, No. 4, 1407–1412, Dec. 1999.